Supplementary Information(SI)

Dissociation of halogenated deoxyuridines as potential radiosensitizers, induced by deep inner-shell photoionization – experiment and modeling.

Kerttu-Inkeri Pusa,[*a] Edwin Kukk,[a] Marta Berholts,[b] Tatiana Marchenko,[c,d] Iyas Ismail,[c,d] Denis Céolin,[d] Marc Simon,[c,d] and Oksana Travnikova[*c,d]

[a] *Department of Physics and Astronomy, University of Turku, FI-20014 Turku, Finland*

[b] *Institute of Physics, University of Tartu, W. Ostwaldi 1, EE-50411 Tartu, Estonia*

[c] *Sorbonne Université, CNRS, UMR 7614, Laboratoire de Chimie Physique-Matière et Rayonnement, F-75005 Paris, France.*

[d] *Synchrotron SOLEIL, L'Orme des Merisiers, Saint-Aubin, F-91192 Gif-sur-Yvette Cedex, France*

[*] *corresponding authors, kerttu.i.pusa@utu.fi, oksana.travnikova@sorbonne-universite.fr*

1 Sample

Organic molecules of the size of 5-iodo-4-thio-2'-deoxyuridine (ISDU) and 5-bromo- 4-thio-2'-deoxyuridine (BrSDU) are susceptible to thermal degradation, which can be a serious issue in thermal evaporation methods that are otherwise best suited for obtaining pure single-molecule targets. Literature data on similar compounds and our complementary home-lab studies show, that the prevalent low-threshold fragmentation channels in gas-phase ionization as well as in radiolysis of the dissolved molecules are (i) rupture of the glycosidic bond, accompanied by hydrogen transfer and (ii), separation of the neutral halogen atom. Below we present the corresponding data specifically for ISDU and BrSDU, demonstrating which are the first bonds to break upon UV ionization. These channels are also expected to be activated in thermal dissociation if it occurs. Because it has not been possible to directly observe the parent molecular ions, some thermally induced degradation of the samples cannot be ruled out. Therefore, our analysis takes this into account by considering also photodissociation processes in 5-iodo-4-thiouracil (ISU) and 5-bromo-4-thiouracil (BrSU), that would be formed by the glycosidic bond breakage and hydrogen transfer from the sugar (D) moiety. The complete separation of the halogen atom, on the other hand, can be ruled out and its occurring contribution identified and efficiently isolated from the data. For example, often-observed contamination of thermally evaporated iodinated samples, I_2 and HI, was observed also in this experiment.

Below we will use the notation ISU for 5-iodo-4-thiouracil ($C_4H_3N_2OSI$, M=254 u), BrSU for 5-bromo-4-thiouracil ($C_4H_3N_2OSIBr$, M=207 u) and SU for thiouracil ($C_4H_3N_2OS$, M=127 u), the fragment from which the halogen atom is separated. D is the sugar moiety after hydrogen transfer ($C_5H_8O_3$, M=116 u) and thus SDU is 4-thio-deoxyuridine with the halogen atom separated (M=243 u). The least-fragmented samples of ISDU and BrSDU were observed in an independent photoelectron-photoion coincidence experiment with 50-eV photon ionization, in the electron binding energy region up to 1 eV above the ionization threshold, as will be investigated in our forthcoming publication. Briefly, Fig. S1 shows that the prominent processes are (a) the glycosidic bond rupturing and (b) halogen-atom separation, accompanied with hydrogen transfer from the sugar to uracil moiety. The latter produces the fragment D of mass 116u for both samples. However, this channel is also mainly accompanied by a water elimination reaction from the sugar moiety, resulting in the, by far the strongest, peak of 98 u. We also observe the thiouracil (SU) and the ISU moieties from ISDU, while for BrSDU, only the the BrSU moiety is detected. For BrSDU, there is a weak signal of what is most likely the SDU-COH fragment, which would be the only fragment with the glycosidic bond intact. With ionization at higher binding energies, the sample fragments more extensively.

Relevant literature data on the specific samples studied here is rare. Evaporated molecular beam of ISDU has been investigated by Saqib *et al.* using electron attachment and mass spectroscopy of

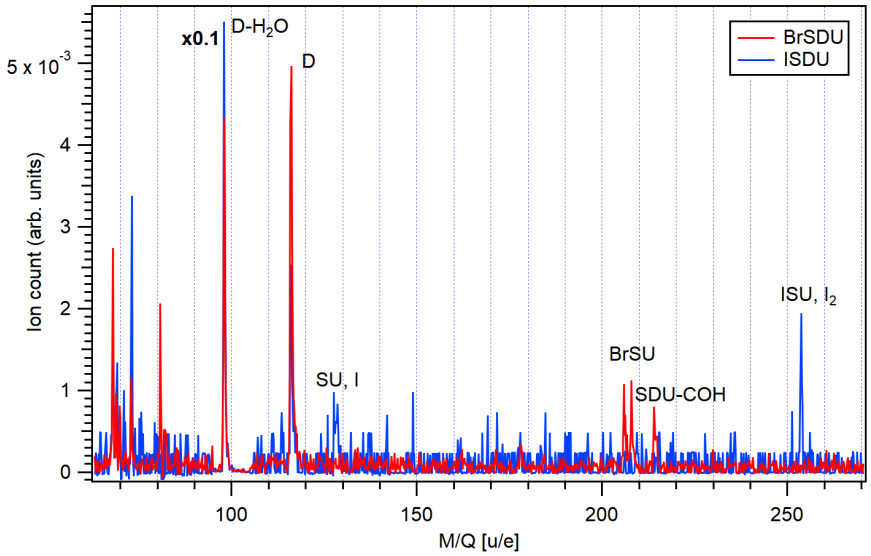

Figure S1: Ion mass spectra of ISDU and BrSDU in coincidence with photoelectrons of less than 9.75 eV binding energy.

anions.[1] The evaporation temperature at that experiment was 110 °C, higher than the 89 °C used in the present work for ISDU. They also carried out an electron impact ionization study of possible thermal degradation of the sample and did not report any. On the other hand, Izadi *et al.*, who studied electron-induced dissociation of 5-bromo-4-thiouracil and BrSDU, observed "... indication of thermal decomposition during the thermal heating process, which leads to ambiguous experimental results" for BrSDU.[2]

As for the related compounds, we have previously studied thermal stability of thymidine (Td) [3, 4], where no thermal degradation was observed until 140 °C. The study also showed the rupture of the glycosidic bond being the characteristic feature of fragmentation dynamics (FD) after UV ionization. Ion mass spectroscopy of thymidine under valence ionization showed that for the undecomposed sample, the glycosidic bond ruptures, which is accompanied by proton transfer from the sugar moiety, so that thymine cations (T^+, m=126 u) are produced. For the present samples ISDU and BrSDU, however, analogous measurements with UV-radiation at home lab did not provide a clear answer on the onset, possibility and degree of thermal decomposition, mostly due to the much more complex dissociation pattern under the UV-ionization itself.

Other means of detecting ongoing thermal decomposition include the observation of signal from the separated neutral halogen atoms, which likely form, in iodine-containing compounds, the HI and I_2 molecules with a very distinctive ion signal. Here, we followed the I_2 contribution over the course of about 9-hour measurement at T=89 °C, and did not observe any increase indicative of an ongoing thermal decomposition – in fact its relative abundancy decreased by 10%. The HI and I_2 molecules, as well as the bromine compounds, can be well isolated in the coincidence data and, in fact, provide a very useful reference. Other possible structural changes, specifically the rupture of the glycosidic bond, are harder to identify and were kept under consideration during the data interpretation and modeling, as the latter was also performed for the ISU and BrSU molecules.

2 Data analysis

2.1 Single-ion data

Some complications in the analysis of spectra from ISDU and BrSDU arise due to the equal or nearly equal M/Q ratios of expected fragments. The atomic N^+ fragments could also be the molecular CH_2^+ fragments. For both O^+ and $^{32}S^{2+}$, M/Q=16 u/e. Although "shadow" features from the

^{34}S isotope with natural abundance of about 4% could be used to determine the contribution from sulfur, the statistics of such features and their overlap with other structures does not permit to use this approach reliably. We therefore assign the associated values jointly to O^+/S^{2+}, although in measurements where the yield of S^+ is very low, it is unlikely that the S^{2+} contribution is significant. In the spectra from ISDU, the $^{32}S^+$ and I^{4+} peaks are separated by only 0.3 u difference, and for BrSDU, as modeling reveals, certain molecular fragments can be produced also in the region of the Br^+ ions.

When analyzing the measured coincidence data some subtractions and corrections were made. Firstly, atomic halogen, or more likely a hydrogen halide, was present in the sample region, likely as a result of thermal degradation. Contribution of I^{n+}- and Br^{n+}-ions from this contaminant was subtracted from the abundances determined from the time-of-flight spectrum. The distinctly low kinetic energy of the contaminant ions was exploited: (i) ions arriving at a radius $R < 5$ mm and (ii) ions that are close, on average $\pm$24 ns and $\pm$30 ns, to the nominal flight time of I^{3+}-I^{10+} and Br^{3+}-Br^{6+} ions, respectively, were filtered out. The narrow peaks in M/Q spectra (main text Figs. 3 and 4) and the narrow, small R patterns in the $R(TOF)$ plots (main text Figs. 5 and 6) arise from the hydrogen halide contamination. It is noteworthy that the two isotopes of bromine, ^{79}Br and ^{81}Br, with nearly equal natural abundances, can not be distinguished from the broadened Br^+ peak, but the doublet peak is distinct in the sharp features arising from the HBr contamination. Br^{3+}, Br^{5+} and Br^{6+} ions' peaks overlap with molecular fragments (MF_A^+), O^+/S^{2+}, and C^+ and N^+ peaks, respectively, from which their contributions were subtracted. Whether or not there are Br^{2+}-Br^{6+} ions originating from BrSDU can not be determined due to the aforementioned overlapping. In the case of Br^{4+}, no ions originating from BrSDU were observed. Secondly, the high-KE iodine ion peaks may contain a contribution from I_2 as an existing contaminant of the sample or a product of possible thermal decomposition that can be isolated efficiently, as discussed below.

2.2 Ion-ion coincidence data

The photoelectron-photoion-photoion coincidence (PEPIPICO) map of ISDU is given in Fig. S2 for the I $2p$ ionization, showing the TOFs of all possible ion pairs from ions detected in individual ionization events that produced the I 2p photoelectrons. In the present context, the PEPIPICO maps are utilized primarily for isolating impurities and for confirming the common molecular parent of the detected individual fragments. The map shows a number of ion-ion coincidence patterns and is dominated by the (C^+,C^+) and (H^+,C^+) coincidences, as statistically expected. The region of the (H^+,H^+) pattern is outside the map – although expected to be strong, the experimental feature is heavily affected by the reduced transmission of the H^+ ions. The PEPIPICO patterns exhibit an average negative slope which stems from the anticorrelation of the ion momenta. Such opposite momenta would strictly arise in the case of a two-body dissociation. The patterns in this case are, however, diffuse and irregular, as expected for a multi-body ICE. Especially the pattern of (C^+,C^+) shows little momentum anticorrelation.

Ion-ion coincidence patterns in the PEPIPICO map and the binding energy shifts of the coincident photoelectronspectra were used in assessing the contribution of I_2. In Fig. S2, narrow patterns marked with a dashed rectangle show a strict momentum anticorrelation of the coincident ions and are assigned to a two-body Coulomb explosion of I_2 after I $2p$ ionization. Further analysis shows that the (I,I) ion pairs have the coincident electron's binding energy 1.0 eV higher than the iodine ions from ISDU due to chemical shift. By analyzing the peak shape of the coincident electrons with each I^{n+} ion of different charge state $n+$, we determined the contribution of I_2 vs. ISDU in each ion peak in the spectum. As a result, the I^+ and I^{2+} ions were fully assigned to ISDU, and the yield of the I^{3+}, I^{4+} and I^{5+} ions had 41(4), 23(3) and 26(3)% contributions by ISDU, respectively. The more highly charged iodine ions were entirely from I_2. However, in the experiment, signal from MF_A^+ and S^+ could also contribute to the I^{5+} and I^{4+} intensities, respectively. In particular, trace amounts of MF_A^+ (likely $C_2H_n{}^+$) can be seen in main text Fig. 5b as a weak left-side contribution to the I^{5+}

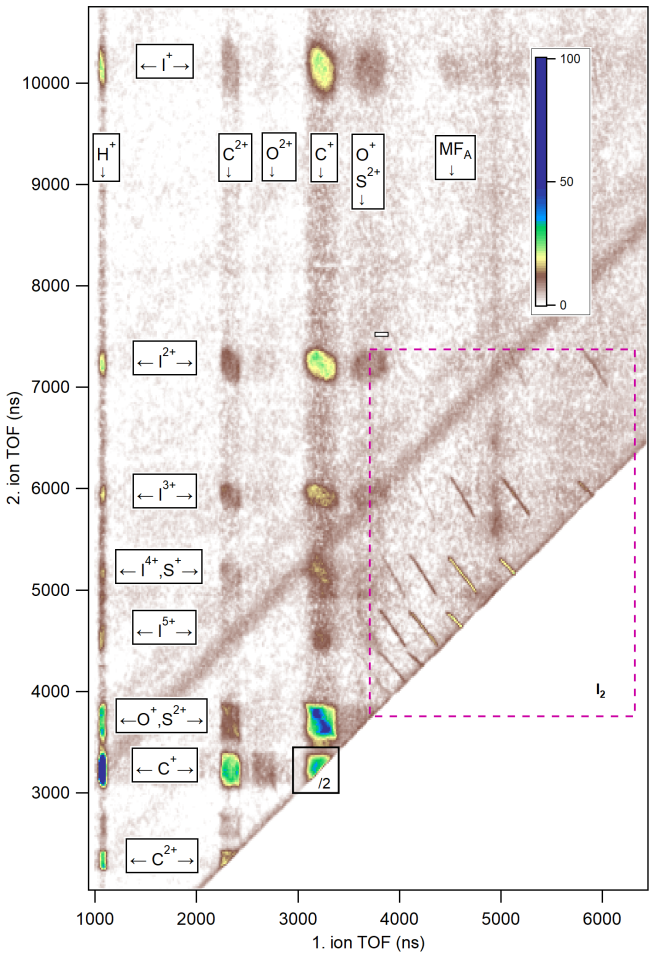

Figure S2: Photoion-photoion coincidence (PIPICO) plot, filtered for the coincident I $2p_{3/2}$ photoelectrons. False coincidence background was subtracted. The dashed rectangle marks the area of two-body dissociation of I_2. Note that the color scale emphasizes weak features, the intensity of the strongest (C^+,C^+) pattern is scaled to 1/2, and the (H^+,H^+) pattern is outside the visible area.

peak. Such molecular fragments are more clearly visible in the case of the S 1s ionization, and are marked in main text Fig. 5a. Their contribution explains the slightly higher assignment of the ISDU sample as the source of I^{5+} ions.

2.3 Hydrogen ions

In the Coulomb explosion of highly charged molecules produced by inner-shell ionization and Auger cascades, protons are ejected with a high kinetic energy (KE) that can seriously compromise their detection, especially under the pulsed extraction field operation mode. Serious distortions are present in the case of I 2p ionization, where their KE is the highest, and the H^+data requires special handling. In the introduction of the MUSTACHE setup [5], we presented ray-tracing simulations of the ion trajectories in the instrument. Such simulations were used here to estimate the transmission (relative fraction of the full 4π solid angle) for detecting $H^+$with a given initial KE.

Simulations showed that under the present experimental settings, the transmission for H^+starts to decrease above 5 eV initial KE, and drops essentially to zero above 25 eV. To correct the observed ion abundances for the reduced transmission, knowledge of their KE is needed, but at high ion losses, its determination from the experiment itself is very unreliable. Instead, we used the ICE simulations by the SPCHMM model (main text Section 4) to obtain the KE distributions of the H^+ions. The simulated H^+ KE distributions were then combined with the ion transmission curve from the ray-tracing simulations. The average transmission (weighted according to the H^+ KE distribution) for the H^+ions was obtained for different ionization conditions and is 0.14, 0.3 and 0.5 for the I 2p ionization in ISDU, the Br 2p ionization in BrSDU and S 1s (ISDU and BrSDU) ionization, respectively. These values were used to correct the abundances in main text Table 1. Nevertheless, due to the high losses, the reported values for $H^+$are much less precise than for the heavier ions.

2.4 Total charge states

In order to estimate the total charge of ISDU following the I 2p ionization, information on I_2 and HI admixtures is useful. The result of their analysis is shown in Fig. S3. The experimental results of this work are compared in Fig. S3 with the calculations of Chaynikov *et al.*[6] for iodine atoms, when the initial vacancy is in the $2p_{3/2}$ and 1s orbitals. Our results for the low-KE iodine ions agree well with those of Chaynikov, although our average charge state of +7.2 e is slightly higher than +6.8 e from the calculation. Note, however, that as the low-energy atomic iodine ions are most likely formed by the dissociation of HI, highly-charged iodine fragments are likely accompanied by a singly charged hydrogen fragment. The experimental total charge as associated with the I $2p_{3/2}$ ionization of HI is therefore likely by +e higher than the distribution shown in Fig. S3. It is also notable, that the calculated distributions for the 1s and $2p_{3/2}$ ionization differ very little, only by 0.2 e as average charge, supporting our premise that the fragmentation patterns following the I $2p_{3/2}$ ionization give a very good representation of the fragmentation following the deepest core ionization of I 1s by, *e.g.*, medical X-rays.

3 Numerical modeling

Tables S1 and S2 present a summary of simulation results in terms of the atomic ion production (ion per a simulation trace) and their average kinetic energy. As an illustration of momentum correlations between two ions, Fig. S4 shows a photoion-photoion coincidence (PIPICO) map for a simulation for ISDU, Q_{tot}=+10 e, that is comparable with the experimental map from I 2p ionization of ISDU in Fig. S2.

Table S1: Simulation results for ISDU and ISU. The energy under "Total" is the kinetic energy release (KER) and for specific ions it is the fragments' average KE. All energies are given in eV. The energy-neutral and energy-gain charge hopping scenarios are marked by "neut." and "gain", respectively. The total of ions/trace is the total yield af atomic fragments, excluding molecular species.

		Atomic ions											
	Total	H^+	C^+	N^+/ CH_2^+	O^+	S^+	I^+	I^{2+}	I^{3+}	C^{2+}	O^{2+}	En. gain	Mol. frag. %
ISDU, Q=10	neut.												
Energy (eV):	163.5	21.6	4.8	7.1	12.6	11.1	4.7	11.8				1.4	24.0
Ions/trace:	7.45	5.82	0.23	0.02	0.16	0.57	0.63	0.01					
ISDU, Q=10	gain												
Energy (eV):	221.8	26.2	9.0	12.1	17.7	11.1	3.0	9.5	14.8	24.2	39.9	68.5	23.6
Ions/trace:	7.67	4.73	1.51	0.12	0.44	0.35	0.49	0.01	0.00	0.02	0.01		
ISDU, Q=5	neut.												
Energy (eV):	30.5	10.0	3.4	4.4	7.4	6.6	4.0					3.8	36.0
Ions/trace:	2.84	1.71	0.00	0.02	0.00	0.47	0.64						
ISDU, Q=5	gain												
Energy (eV):	65.5	13.1	3.6	4.4	8.1	4.8	2.1	11.4				59.0	36.3
Ions/trace:	3.10	2.38	0.23	0.02	0.08	0.13	0.26	0.0004					
ISU, Q=10	neut.												
Energy (eV):	240.0	33.1	16.6	22.6	32.4	24.0	7.5	12.4	15.4			-5.8	3.8
Ions/trace:	6.97	2.14	1.40	0.35	0.59	1.20	0.87	0.40	0.02				
ISU, Q=10	gain												
Energy (eV):	268.0	37.5	20.7	26.1	30.8	20.7	5.8	9.8	13.8	33.4	60.8	9.2	2.9
Ions/trace:	8.77	2.14	2.93	1.12	0.62	0.74	0.67	0.22	0.01	0.27	0.05		
ISU, Q=5	neut.												
Energy (eV):	41.0	12.3	3.04	5.0	8.2	7.2	3.6					-5.6	29.2
Ions/trace:	3.54	1.72	0.17	0.03	0.06	0.72	0.84						
ISU, Q=5	gain												
Energy (eV):	58.7	16.4	4.6	7.3	12.98	7.2	2.6	3.6			11.6	16.7	23.7
Ions/trace:	3.8	1.43	0.94	0.19	0.21	0.44	0.58	0.003			0.01		

Table S2: Simulation results for BrSDU and BrSU. The energy under "Total" is the kinetic energy release (KER) and for specific ions it is the fragments' average KE. All energies are given in eV. The energy-neutral and energy-gain charge hopping scenarios are marked by "neut." and "gain", respectively. The total of ions/trace is the total yield af atomic fragments, excluding molecular species

		Atomic ions												
	Total	H^+	C^+	N^+/ CH_2^+	O^+	S^+	Br^+/ MF	Br^{2+}	Br^{3+}	C^{2+}	O^{2+}	S^{2+}	En. gain	Mol. frag. %
BrSDU, Q=6	neut.													
Energy (eV):	46.8	11.9	3.8	4.9	7.6	6.7	5.4	12.8				15.6	1.9	33.5
Ions/trace:	3.63	2.82	0.01	0.02	0.01	0.57	0.20	0.001				0.01		
BrSDU, Q=6	gain													
Energy (eV):	87.5	15.6	4.4	6.0	10.0	5.7	3.4	5.9		19.2	34.6	19.2	60.5	36.5
Ions/trace:	3.82	2.88	0.51	0.03	0.12	0.19	0.09	0.002		0.001	0.001	0.001		
BrSDU, Q=5	neut.													
Energy (eV):	28.4	9.9	4.2	4.6	6.3	6.2	4.9	9.5				14.1	0.07	39.3
Ions/trace:	2.59	1.83	0.001	0.01	0.01	0.56	0.19	0.001				0.001		
BrSDU, Q=5	gain													
Energy (eV):	64.5	13.3	3.6	5.3	8.3	4.8	3.0	1.1		4.5			56.5	40.3
Ions/trace:	2.99	2.39	0.32	0.02	0.06	0.14	0.06	0.001		0.001				
BrSU, Q=6	neut.													
Energy (eV):	69.4	17.0	4.1	7.0	13.4	9.8	6.1	10.7		4.8		24.3	-1.1	27.9
Ions/trace:	4.32	1.82	0.98	0.20	0.24	0.72	0.36	0.004		0.002		0.002		
BrSU, Q=6	gain													
Energy (eV):	87.7	20.5	6.3	9.9	16.0	9.4	4.9	8.1	5.2	13.9	19.0	15.4	18.1	20.2
Ions/trace:	4.76	1.65	1.54	0.37	0.31	0.57	0.29	0.01	0.001	0.02	0.003	0.01		
BrSU, Q=5	neut.													
Energy (eV):	44.2	13.3	2.7	5.4	8.7	7.1	4.5	12.1				14.3	0.09	32.7
Ions/trace:	3.36	2.01	0.27	0.04	0.09	0.65	0.30	0.002				0.002		
BrSU, Q=5	gain													
Energy (eV):	57.7	16.0	4.1	6.8	12.7	6.7	4.3	8.6		16.1	34.4	12.0	16.4	30.1
Ions/trace:	3.49	1.47	0.98	0.22	0.19	0.46	0.16	0.002		0.01	0.001	0.002		

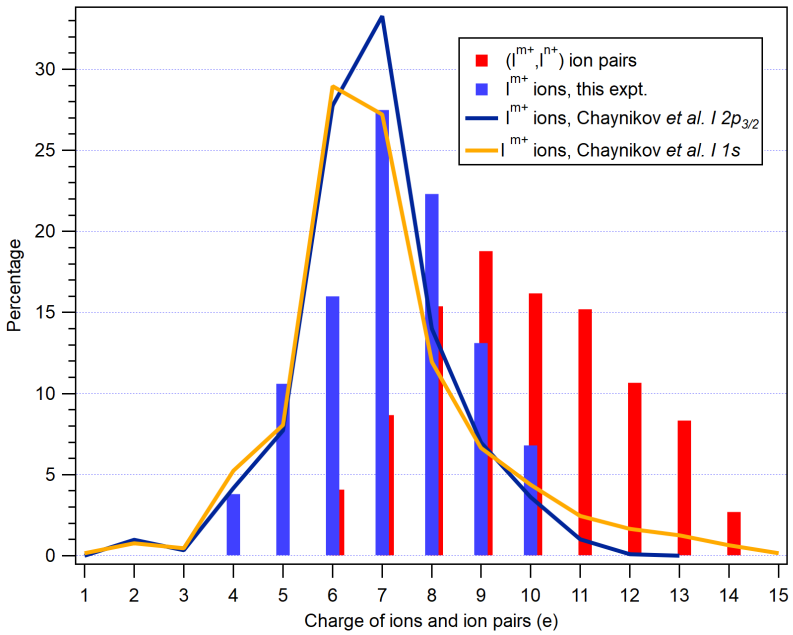

Figure S3: Charges of high-KER (I^{m+},I^{n+}) ion pairs and of single low-KE I^{m+} ions. The former are extracted using intensities of the well-defined ion-ion coincidence patterns in the PEPIPICO maps in coincidence with the I $2p_{3/2}$ photoelectron. The latter are filtered from the $R(TOF)$ maps of ions in coincidence with the I $2p_{3/2}$ photoelectrons. Solid lines show theoretical results by Chaynikov *et al.*, Ref. 6.

References

[1] M. Saqib, E. Arthur-Baidoo, F. Izadi, A. Szczyrba, M. Datta, S. Demkowicz, J. Rak and S. Denifl, *J. Phys. Chem. Lett.*, 2023, **14**, 8948–8955.

[2] F. Izadi, A. Szczyrba, M. Datta, O. Ciupak, S. Demkowicz, J. Rak and S. Denifl, *International Journal of Molecular Sciences*, 2023, **24**, 8706.

[3] H. Levola, K. Kooser, E. Rachlew, E. Nõmmiste and E. Kukk, *International Journal of Mass Spectrometry*, 2013, **353**, 7–11.

[4] H. Levola, K. Kooser, E. Itälä and E. Kukk, *International Journal of Mass Spectrometry*, 2014, **370**, 96–100.

[5] E. Kukk, R. Vacheresse, I. Ismail, T. Marchenko, R. Guillemin, M. N. Piancastelli, M. Simon and O. Travnikova, *J Synchrotron Rad*, 2025, **32**, 1017–1027.

[6] A. P. Chaynikov, A. G. Kochur and A. I. Dudenko, *Phys. Scr.*, 2024, **99**, 045407.

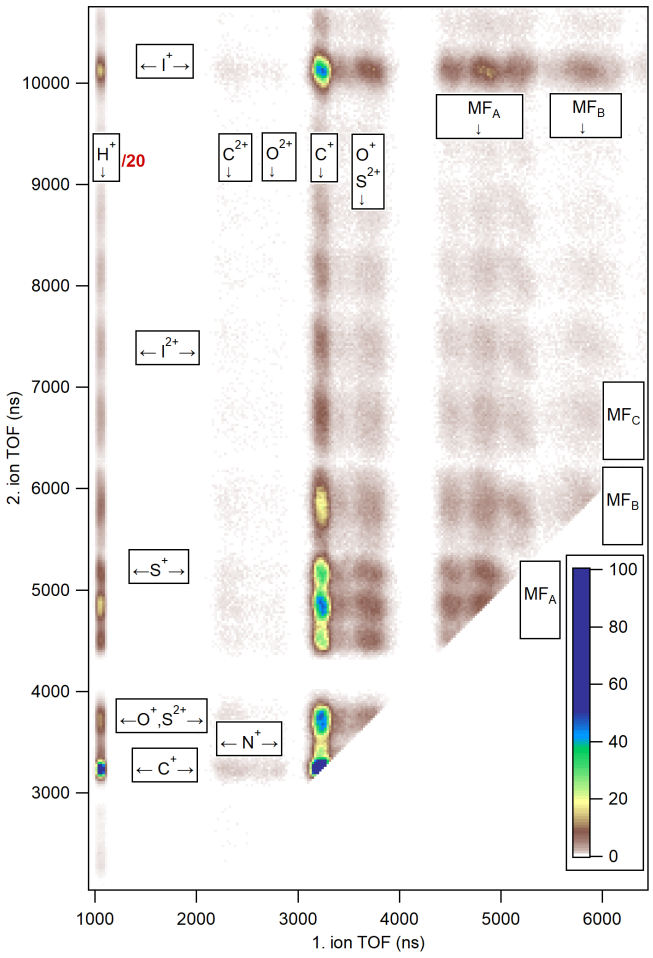

Figure S4: Simulated PIPICO plot of ISDU, with Q_{tot}=+10e using the energy-neutral charge hopping scenario. The map is composed of all the charged fragment pair combinations in the events represented by 50000 calculated trajectories. The fragment masses-to-charge ratios and momenta were converted to the ion TOFs using the spectrometer's parameters for this experiment.